

Coronal Hole and Solar Global Magnetic Field Evolution in 1976 – 2012

Irina A. Bilenko¹ · Ksenia S. Tavastsherna² ·

© Springer ●●●

Abstract Coronal hole spatial-temporal evolution is studied and comparison made with that of the solar global magnetic field in cycles 21–23 (1976–2012). The latitude-longitude distribution dynamics of coronal holes and the regularities in the global magnetic field associated with the solar polar field reversal are analyzed. Polar and non-polar coronal hole populations are considered. The investigation reveals some temporal and spatial regularities in coronal hole distributions that match well the global magnetic-field cycle evolution. The results show that the non-polar coronal hole longitudinal distribution follows all configuration changes in the global magnetic-field structure. Reorganizations of the global magnetic-field and coronal hole distributions occur simultaneously during a time interval of a few solar rotations. The cycle evolution of the non-polar coronal holes reflects the transition of the solar global magnetic field from the zonal structure to sectorial and *vice versa*. Two different type waves of non-polar coronal holes are revealed from their latitudinal distribution. The first one is short poleward waves. They trace the poleward motion of the unipolar photospheric magnetic fields from approximately 35° to the associated pole in each hemisphere and the redevelopment of a new-polarity polar CH. Although they start the poleward movement before the change of the polar magnetic field in the associated hemisphere, they reach the pole after the polar reversal. The other type of non-polar CH wave forms two sinusoidal branches associated with the positive- and negative-polarity magnetic fields. The complete period of the wave was equal to ≈ 268 CRs (22 years). These wave CHs arrive at high latitudes during declining phases when the new polarity polar CHs are already completely formed.

Keywords: Magnetic fields, Corona; Coronal Holes; Solar Cycle, Observations;

¹ Moscow M.V. Lomonosov State University, Sternberg Astronomical Institute, Universitetsky pr.13, Moscow, 119992, Russia, email: bilenko@sai.msu.ru

² Central (Pulkovo) Astronomical Observatory, Russian Academy of Sciences, Pulkovskoe sh. 65, St. Petersburg, 196140, Russia

1. Introduction

Coronal holes (CHs) are regions of low radiation in the extreme ultraviolet and X-ray wavelengths in the solar atmosphere. The study of CHs is important in view of their role in the space weather formation at the Earth's orbit and their influence on geomagnetic activity. CHs are associated with open magnetic field structures in the solar atmosphere and they are considered to be the source of high-speed solar wind (Nolte *et al.*, 1976; Obridko, Shelting, and Livshits, 2011; Bilenko, 2005; Tlatov, Tavastsherna, and Vasil'eva, 2014). CHs are mainly located on unipolar magnetic fields with one predominant polarity (Bohlin and Sheeley, 1978; Bumba, Klvařna, and Sýkora, 1995; Harvey, Sheeley, and Harvey, 1982; Timothy, Krieger, and Vaiana, 1975; Varsik, Wilson, and Li, 1999). Tavastsherna and Polyakow (2014) found that 70% of CHs were located in unipolar regions. The unipolarity degree of the photospheric magnetic field in CH regions is 0.1–0.3 (Tavastsherna and Tlatov, 2004). CHs are associated with low photospheric magnetic fields $\approx 1-5$ G, but they are located at the hills of the coronal magnetic field (Obridko and Shelting, 1989; Tavastsherna and Tlatov, 2004). Approximately 85% of CHs are entirely or partly located in the regions of maximum coronal field intensity for a given rotation (Obridko and Shelting, 1989). The average size of the photospheric magnetic elements of dominant polarity and their parameters such as magnetic-field strength, magnetic flux, and magnetic flux imbalance in CH regions differ from that in “quiet” regions and the differences increase with solar activity cycle (Belenko, 2001). Since CHs are located in regions with a pronounced dominance of one of the polarities of the solar magnetic field, the changes in their distribution over the solar disk can be used as good tracers of evolutionary changes in the associated positive- and negative-polarity magnetic field.

As shown by Ivanov and Obridko (2014), the large-scale structure of the solar magnetic field determines the global organization of almost all solar activity phenomena, such as active regions, filaments, CHs, and coronal mass ejections. It was found that the time-space distribution of CHs on the solar disk is not uniform. They form some cluster structures. The complexity of the structures and the life-time of individual clusters depend on the solar cycle phase (Bilenko, 2004b). It was also found that the longitudinal distribution of positive- and negative-polarity CHs match well to that of the solar global magnetic field (GMF) in Cycle 23 (Bilenko, 2012). Wang and Sheeley (1990) noted that the topology of CHs is determined by that of the unipolar regions in which they are embedded.

CHs can be divided into two groups: polar and non-polar CHs according to their latitudinal location on the solar disk (Sanchez-Ibarra and Barraza-Paredes, 1992). Their number, latitude distribution, rotation, and cycle evolution are different (Insley, Moore, and Harrison, 1995). Polar CHs have a maximal area at the minimum phase of a solar cycle (Bravo and Stewart, 1997; Dorotovič, 1996; Harvey and Recely, 2002; Hess Webber *et al.*, 2014). During the rising phase polar CHs shrink and they disappear completely about one to two years before the sunspot maximum (Waldmeier, 1981). At the maximum phase, the polar magnetic fields change their polarities and new-polarity polar CHs are created

at the solar poles (Webb, Davis, and McIntosh, 1984; Fox, McIntosh, and Wilson, 1998; Harvey and Recely, 2002, Bilenko, 2002). The total number and area of non-polar CHs increase with the solar cycle progression from the minimum to the maximum phase (McIntosh, Thompson, and Willock, 1992; Belenko, 2001; 2002). It was found that the long-lived non-polar CHs have approximately the same differential rotation as sunspots, and long-lived polar CHs show a rigid rotation (Ikhsanov and Ivanov, 1999). Polar and low-latitude CHs have different plasma parameters (Miralles, Cranmer, and Kohl, 2001, 2002, 2006). Polar CH cycle evolution is closely connected to the polar magnetic fields, which confirms that global processes are involved (Fox, McIntosh, and Wilson, 1998). Ikhsanov and Tavastsherna (2015) showed that large CHs associated with high-latitude large-scale magnetic fields and low-latitude small CHs that appear as a result of decaying local sunspot fields formed two magnetic field systems, that evolve in antiphase with respect to one another, with a shift in their minima by $\approx 5-6$ years.

Non-polar and polar CHs can also be divided into two subclasses, based on CH area behavior at various phases of a solar cycle, on their latitude and longitude distribution, rotation, and life-time as shown by Ikhsanov and Ivanov (1999). They also found that at the rising and maxima phases, the CH magnetic fields are of quadrupole type and at the declining and minima phases they are of dipole type. The period of quadrupole magnetic field coincides with the epoch of more rigid equatorial CH rotation because of high-latitude CH emergence. It was shown that the low-latitude long-lived CHs possess differential rotation that is similar to that of sunspot groups, and the long-lived polar CHs revealed a rigid rotation (Ikhsanov and Ivanov, 1999).

Occurrence and cycle evolution of CHs depend also on their association with active regions or GMF (Bilenko, 2004a). Active-region CHs are closely connected to the processes occurring in the active regions. CHs which are not connected to active regions reflect the distribution of large-scale solar magnetic fields determined by the GMF cycle evolution from zonal structure at the solar minimum to sectorial at the maximum when an alternation of longitudes covered by opposite-polarity CHs is observed (Bilenko, 2002). The power spectra of CH numbers have periods of 13, 27, and 160 days. These are the same periods which are detected for other solar activity phenomena. They reflect the two and four sectorial structures of the GMF (Belenko, 2001). Bumba, Klvaňa, and Sýkora (1995) found that two opposite longitudinal rows of equatorial CHs located approximately 180° apart existed in 1991. They concluded that the formation of CHs at each such active longitude was a global process, and that this process depends on the development and distribution of background and local magnetic fields and on the phase of the cycle. The nine-day period recurring for several solar rotations, revealed in solar wind parameters, is also the manifestation of the periodic longitudinal distribution of CHs on the Sun (Temmer, Vršnak, and Veronig, 2007).

The aim of this work is to analyze the spatial and temporal distributions of CHs on the solar disk, their relation to the solar polar magnetic-field reversal and to compare them to that of the GMF during 1976–2012. An understanding of the observed CH and GMF cycle spatial-time evolution should provide some insight into the nature of solar cycle formation and dynamics.

Section 2 describes the data used. In Section 3, the spherical harmonic description of the solar GMF is presented. CH latitudinal distribution in cycles 21–23 is analyzed in Section 4. The longitudinal distributions of CHs and the GMF are investigated in Section 5. The comparison of CH parameters and GMF is made in Section 6. The main conclusions are listed in Section 7.

2. Data

The CH catalog of the Solar Kislovodsk Mountain Astronomical Station of Pulkovo Observatory was used. The catalog includes data on CH locations: latitude and longitude and CH parameters such as CH extension in latitude and longitude, area, associated photospheric magnetic-field strength (in G) and polarity, and magnetic flux. The detailed description of the method used for CH definition, CH parameter determination, and the catalog creation are described in Tlatov, Tavastsherna, and Vasil’eva (2014).

To compare the solar GMF and CH evolution at different phases of solar cycles 21–23, we use data on the daily photospheric large-scale magnetic fields and calculated coronal magnetic fields from the Wilcox Solar Observatory (WSO) for the years 1976–2012. Daily photospheric magnetograms are full-disk maps of the line-of-sight component of magnetic flux at the photosphere. The line used is the 5250 Å absorption line of neutral iron (Fe I). The coronal magnetic field is calculated from photospheric fields with a potential field model with the source-surface location at $2.5 R_{\odot}$ (Schatten, Wilcox, and Ness, 1969; Altschuler and Newkirk, 1969, 1975; Hoeksema; Hoeksema and Scherrer, 1986, 1988). Source-surface magnetic-field data consist of 30 data points in equal steps of sine latitude from $+70^{\circ}$ to -70° . Longitude is presented in 5° intervals. Full-disk synoptic map data span a full Carrington Rotation (1 CR = 27.2753 days). The entire data set consists of 488 synoptic maps and covers CRs 1642–2130 (June 1976–November 2012).

Daily coronal hole maps in the $\lambda = 10830 \text{ \AA}$ line of the Kitt Peak NSO, SOHO/EIT (Solar and Heliospheric Observatory/Extreme ultraviolet Imaging Telescope) (Delaboudinière *et al.*, 1995) images in the $\lambda = 284 \text{ \AA}$ line, and *Yohkoh*/SXT (Soft X-ray Telescope) (Tsuneta *et al.*, 1991) images were used for illustrations.

3. Spherical Harmonic Description of the Solar Global Magnetic Field

We use spherical harmonic analysis to investigate the solar GMF cycle evolution during 1976–2012. The magnetic field can be described as a function of latitude and longitude coordinates (r, θ, ϕ) by the potential function (Altschuler and Newkirk, 1969; Altschuler *et al.*, 1975; Altschuler *et al.*, 1977; Chapman and Bartels, 1940):

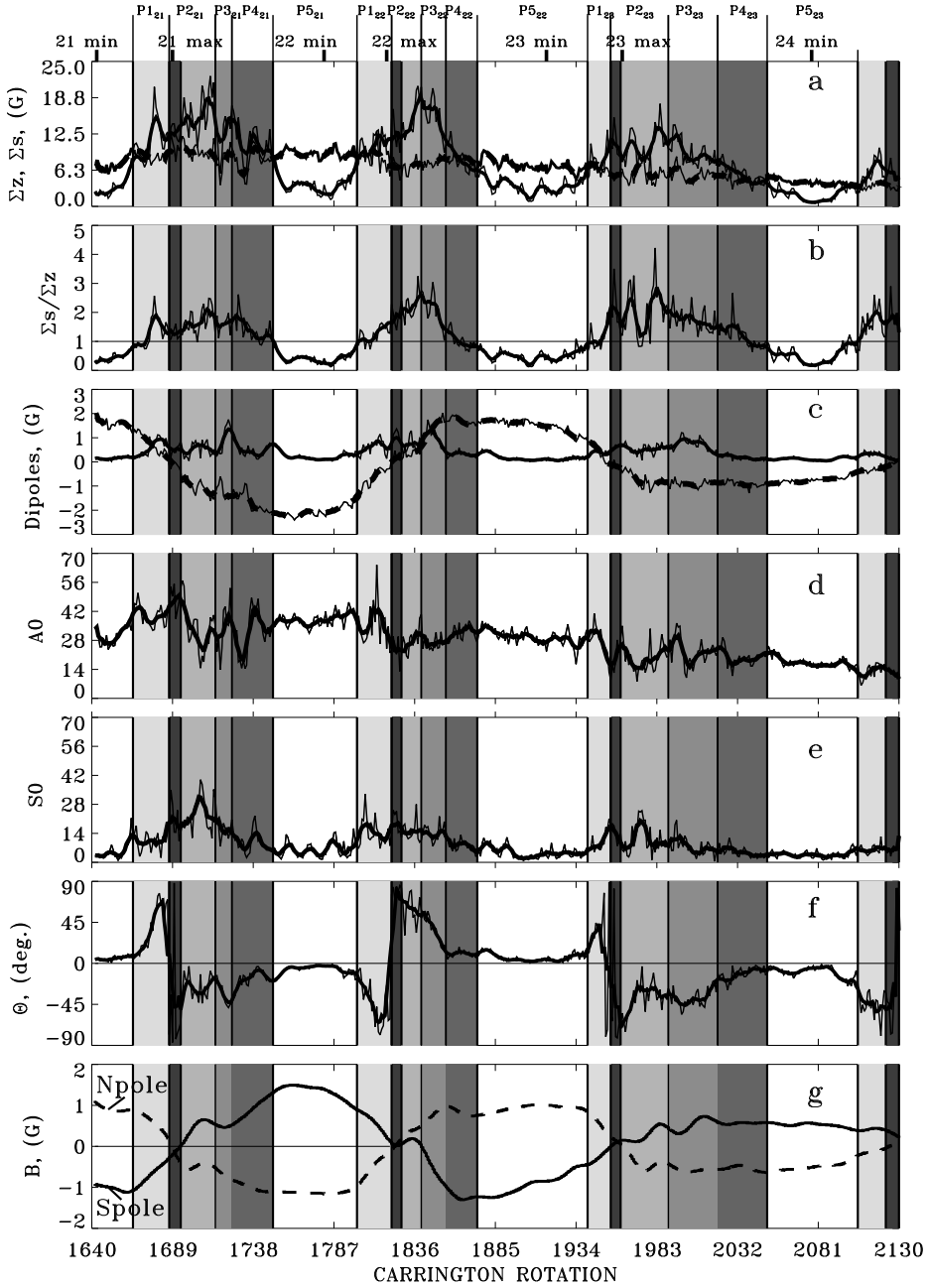


Figure 1. (a) Sectorial harmonic spectra sum (solid line) and that of zonal harmonics (dashed line); (b) the ratio of the sectorial harmonic sum to the zonal harmonic sum; (c) dipole components: axisymmetric dipole (dashed line) and equatorial dipole (solid line); (d) the axisymmetric, and with respect to the equator, antisymmetric harmonic spectra sum; (e) the axisymmetric, but symmetric with respect to the equator, harmonic spectra sum; (f) the polar angle, θ , of the dipole component; (g) polar magnetic-field evolution in the northern and southern hemispheres. Thin lines correspond to CR-averaged and thick lines represent seven CR-averaged data. Light-, mid-, and dark-grey mark the P1–P4 periods of the sectorial GMF structure domination. Black indicates a magnetic-field polarity reversals at the North and South poles.

$$\psi(r, \theta, \phi) = R \sum_{n=1}^N \sum_{m=0}^n \left(\frac{R}{r}\right)^{n+1} [g_n^m \cos(m\phi) + h_n^m \sin(m\phi)] P_n^m(\theta),$$

where $P_n^m(\theta)$ are the associated Legendre polynomials, and N is the number of harmonics. The coefficients g_n^m , h_n^m are calculated using a least mean-square fit to the observed line-of-sight photospheric magnetic fields with a potential field assumption. The harmonic power spectra can be calculated (Altschuler *et al.*, 1977; Levine, 1977) using

$$S_n = \sum_{m=0}^n [(g_n^m)^2 + (h_n^m)^2].$$

The sectorial harmonic spectra sum (solid line) and that of zonal harmonics (dashed line) are presented Figure 1a. In cycle 23, the sectorial components have a long “tail”. The ratio of the sectorial to zonal harmonic sum is presented in Figure 1b. The horizontal line marks the level where the sum of the sectorial harmonics is equal to that of the zonal harmonics.

The temporal evolution of the axisymmetric harmonic component of the solar dipole g_1^0 (dashed line) and that of the equatorial dipole (solid line)

$$S_{eqv.dip.} = \sqrt{(g_1^1)^2 + (h_1^1)^2}$$

are shown in Figure 1c.

In Figure 1d, the axisymmetric, and with respect to the equator, antisymmetric harmonic spectral sum (Stix, 1977) is shown:

$$A0 = \sum_{n=1,3,5} (n+1)g_n^0 P_n(\theta).$$

In Figure 1e, the axisymmetric, but symmetric with respect to the equator, harmonic spectra sum (Stix, 1977) is presented:

$$S0 = \sum_{n=2,4,6} (n+1)g_n^0 P_n(\theta).$$

The polar angle, θ , of the dipole component evolution is shown in Figure 1f:

$$\tan \theta = (g_1^0)^{-1} [(g_1^1)^2 + (h_1^1)^2]^{1/2}.$$

The observed North pole (dashed line) and South pole (solid line) magnetic-field variations are shown in Figure 1g. The maxima and the minima of cycles 21–24 are marked at the top of Figure 1.

For further investigation and comparison of the GMF and CHs, different periods are selected in each cycle according to the GMF harmonic spectra and

GMF structure (Figures 1, 3). The first periods ($P1_{21} - P1_{23}$) are the time from the beginning of the sectorial structure domination to the beginning of the polar magnetic-field sign changes in each cycle. During the first period, the polar magnetic-field strength, zonal harmonic spectra sum, and axisymmetric component of the solar dipole decreased. The sectorial components increased. The non-axisymmetric component of the GMF, $A0$, was at the highest level in each cycle. The axisymmetric component of the GMF, $S0$, increased, and the inclination of θ increased rapidly.

Periods $P2_{21} - P2_{23}$ and $P3_{21} - P3_{23}$ are defined as being from the beginning of the polar magnetic-field sign changes to the end of two-sectorial structure domination (Figure 3), when the sum of sectorial components becomes approximately equal to that of zonal components, and θ reaches a minimal value. During these periods the sectorial structure dominates. The axisymmetric component of the solar dipole changes sign and begins to increase in each cycle. The non-axisymmetric component of the GMF ($A0$) reaches a minimum, and the axisymmetric component of the GMF ($S0$) increases to a maximum. The magnetic field at the poles changes sign and begins to increase. The polar angle, θ , reaches the highest latitudes and begins to decline.

The periods ($P4_{21} - P4_{23}$) last until the end of the sectorial structure domination in each cycle. During these periods the magnitude of sectorial components diminishes and that of the zonal components increases. The axisymmetric component of the dipole and the polar magnetic-field strength increase. The non-axisymmetric component of the GMF ($A0$) increases slightly, and the axisymmetric component of the GMF ($S0$) decreases. The polar angle, θ , is reduced to zero.

The periods ($P5_{21} - P5_{23}$) are characterized by the zonal GMF structure domination. The polar magnetic-field strength and the axisymmetric component of the solar dipole reach a maximum. The axisymmetric component of the GMF ($S0$) is at the lowest level. The polar angle, θ , is close to zero. In Figure 1, the periods are marked in light-, mid-, and dark-grey. Black indicates magnetic-field-polarity sign changes at the North and South poles.

The sectorial and zonal harmonic spectral sum, the magnitude of axisymmetric component of the solar dipole, $A0$, $S0$, and the North and South polar magnetic-field strength diminish from cycle 21 to cycle 23.

4. Latitudinal Distribution of Coronal Holes

Figure 2 presents (a) the latitudinal distribution of positive-polarity (red) and negative-polarity (blue) CHs and (b) North and South polar magnetic fields in 1975–2012. The maxima and minima of cycles 21–24 are marked at the top of Figure 2.

CHs are clearly divided into two groups: polar and non-polar CHs, according to their latitudinal locations. Thick horizontal lines at $\pm 55^\circ$ latitudes separate the two groups.

The two different type waves of non-polar CHs can be detected from their latitudinal distribution shown in Figure 2. The first one (waves 1) are short

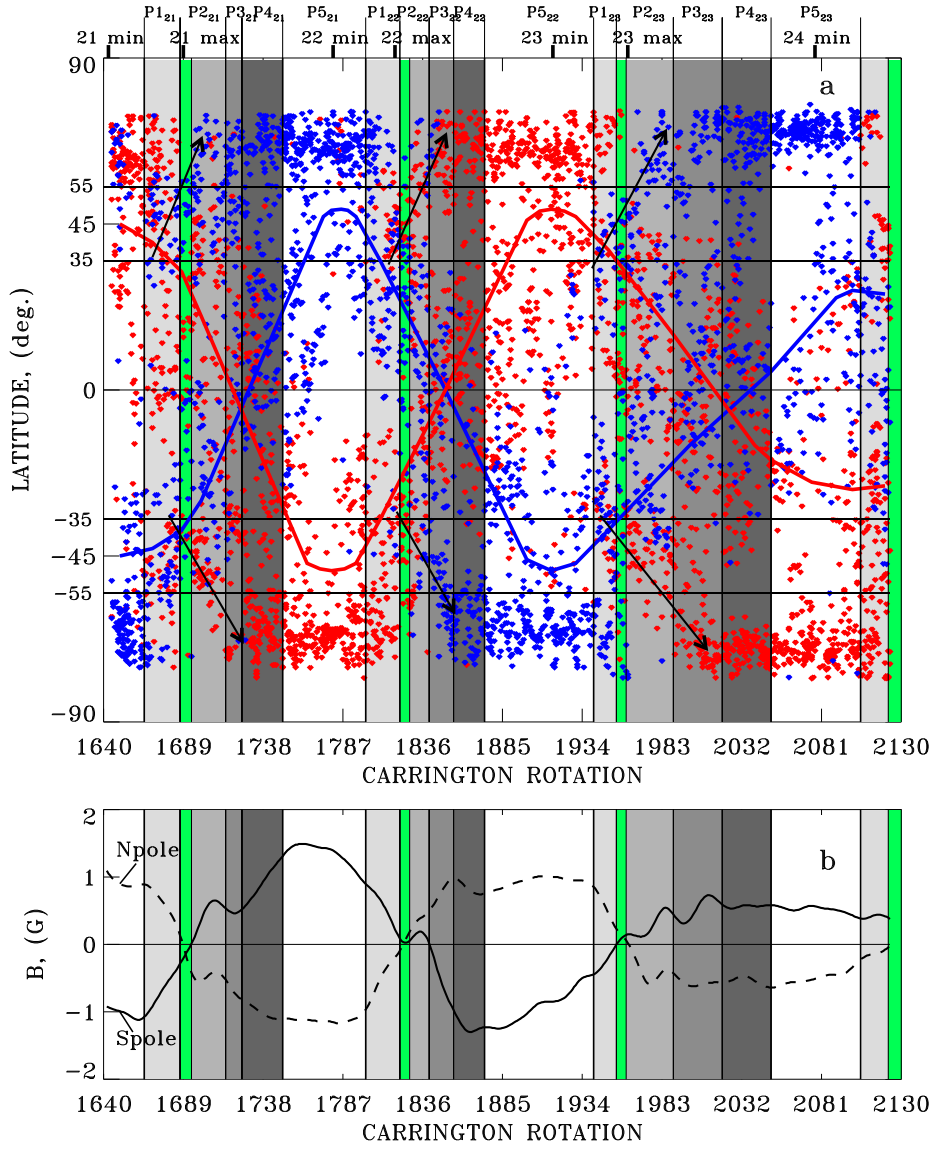


Figure 2. (a) The latitudinal distribution of CHs in 1975–2012; (b) polar magnetic-field evolution in the northern and southern hemispheres. Red denotes the CHs associated with the positive-polarity photospheric magnetic fields and Blue denotes the CHs associated with the negative-polarity photospheric magnetic fields. Light-, mid-, and dark-grey mark the P1–P4 periods of the sectorial GMF structure domination. Green indicates magnetic-field polarity reversals at the North and South poles.

poleward waves that are marked by black arrows. They indicate new-polarity CHs traveling from approximately 35° to the associated pole in each hemisphere. Ikhsanov and Tavastsherna (2013) also found that the large-area (>15000 millionths of the solar hemisphere) high-latitude CHs and polar faculae rose from midlatitudes ($40^\circ - 50^\circ$) to the polar regions. The rise was in the form of several slanted chains about a half-year width in time and with a periodicity of 1.25 ± 0.3 years in cycle 21. They noted that the CH polarity corresponded to the trailer polarity of active regions.

The other type are non-polar CH waves (waves 2) that form two sinusoidal branches. One branch is associated with the positive-polarity magnetic fields (red line) and the other with that of the negative-polarity (blue line). Wave 2 CHs associated with the positive- and negative-polarity magnetic fields are in antiphase in each cycle. The latitude-location cycle changes of the wave 2 CHs coincide with that of the axisymmetric component of the solar dipole (g_1^0), as shown in Figure 1c. Wave 2 CH branches and the axisymmetric component of the solar dipole are the lowest in cycle 23, where they do not exceed latitudes $\pm 35^\circ$. The complete period of the wave 2 is equal to ≈ 268 CRs (≈ 22 years). Since CHs are located in solar atmospheric regions with a dominance of one of the magnetic-field polarities, the changes in their distribution over the solar disk is the manifestation of evolutionary cycle changes in the solar magnetic fields. When two branches of positive- and negative-polarity magnetic fields, traced by wave 2 CHs, move below $\approx \pm 35^\circ$ in latitude, the sectorial structure of the GMF is established. Unipolar CH longitudes are formed, which are occupied by only positive or by only negative-polarity CHs alternated approximately with a period of 13 days and covering $\approx 60 - 100^\circ$ of longitude (Bilenko, 2002). When both wave 2 polarity branches are located higher than $\approx \pm 35^\circ$ and reach the highest latitudes in each hemisphere, the zonal GMF structure was observed. The polarity of CH-associated magnetic fields matches the polarity of the polar regions in the associated hemisphere at that time.

The CH evolution during a solar cycle is closely related to solar polar magnetic-field reversals (Fox, McIntosh, and Wilson, 1998; Webb, Davis, and McIntosh, 1984; Harvey and Recely, 2002). Webb, Davis, and McIntosh (1984) studying the evolution of the polar magnetic field around sunspot maximum and polar CH redevelopment in cycles 21 and 22 and found that the process of polar field reversals and redevelopment of the polar CHs was discontinuous and occurred in two or three longitudinal bands, and an asymmetry of the processes in opposite hemispheres was revealed. The polarity reversals in the two hemispheres were offset between six months to one and a half years. Harvey and Recely (2002) found that new-polarity CHs formed in the remnants of the follower active region magnetic fields before the polar reversal and expanded to cover the poles within three solar rotations after the polar reversal in cycles 22 and 23. During the first 1.2–1.4 years polar CHs were asymmetric (Harvey and Recely, 2002).

From Figure 2 it is seen that wave 2 CHs are not associated with that process. They arrive at high latitudes when the polar CHs of a new polarity have already completely formed. Even more, they reach the highest latitudes and the locations of polar CH regions during the late decline phase. The wave 2 CHs reach the

highest latitudes during the period of the zonal GMF structure domination (P5₂₁–P5₂₃).

As seen in Figure 2a, the wave 1 CHs form before the polar magnetic-field reversal in each cycle. The polarity of the wave 1 CHs corresponds to the trailer polarity of active regions and, correspondingly, to the leading polarity of the next cycle (Figure 2a). The waves 1 began ≈ 16 and ≈ 8 CRs before the polar magnetic-field sign changes in the North and South pole correspondingly in cycle 21, ≈ 10 and ≈ 3 CRs in cycle 22, and ≈ 20 and ≈ 18 CRs in cycle 23. The first CHs with the polarity of the polar CH waves appear around the time of the beginning of the sectorial stricture domination, the first period (P1₂₁–P1₂₃), in each cycle. The waves are asymmetric in the North and South hemispheres. The longest waves 1 are seen in cycle 23. Wave 1 CHs trace the poleward motion of the unipolar photospheric magnetic fields to the polar regions and the redevelopment of a new-polarity polar CH. Wave 1 CHs and magnetic flux start a poleward movement before the change of the polar magnetic field in the associated hemisphere, but they reach the pole after the reversal. They reach the pole region and the main new-polarity polar CHs are formed at the pole regions just after the polar magnetic-field sign changes at the North pole in cycles 21, 22 and in ≈ 20 CRs after the polar field reversal at the North pole in cycle 23, and approximately 40, 27, and 38 CRs after the polar magnetic-field polarity changes at the South poles in cycles 21, 22, and 23 correspondingly. It should be noted, that some old-polarity polar CHs are observed at the time of the polar field reversals and up to ≈ 20 CRs after the polar magnetic-field sign changes. The episodic new-polarity CHs are observed ≈ 10 – 15 CRs before the polar field reversal at the polar CH latitudes.

Polar CHs are arranged more compactly in cycle 23, and they are located in a wider range of latitudes in cycles 21 and 22.

5. Longitudinal Distribution of Coronal Holes and the Solar Global Magnetic Field

In Figure 3a, the longitudinal distribution of non-polar CHs is presented and in Figure 3b, the time-longitude distribution of the strength and polarity of GMF from -55° to $+55^\circ$ latitudes is shown. The longitudinal diagram was created in a CR-rotation system. The x -axis denotes the date of 0° CR longitude at the central meridian, and the y -axis denotes longitude. A detailed description of the longitudinal diagram creation and GMF changes is given in Bilenko (2014). The maxima and minima of the cycles are marked at the top of Figure 3. The comparison of the CH and GMF longitudinal distributions shows that the CH cluster structure (Bilenko, 2004b) completely coincides with the GMF longitudinal distribution. Positive-polarity CH locations coincide with positive-polarity (red) GMF and negative-polarity CH locations coincide with negative-polarity (blue) GMF. CH longitudinal distributions follow all configurations in the GMF. Quasi-stable two-polarity GMF structures match well to the positive- and negative-polarity CH locations at the solar maxima and at the beginning of the declining phases. Drifts in the GMF during the rising and declining

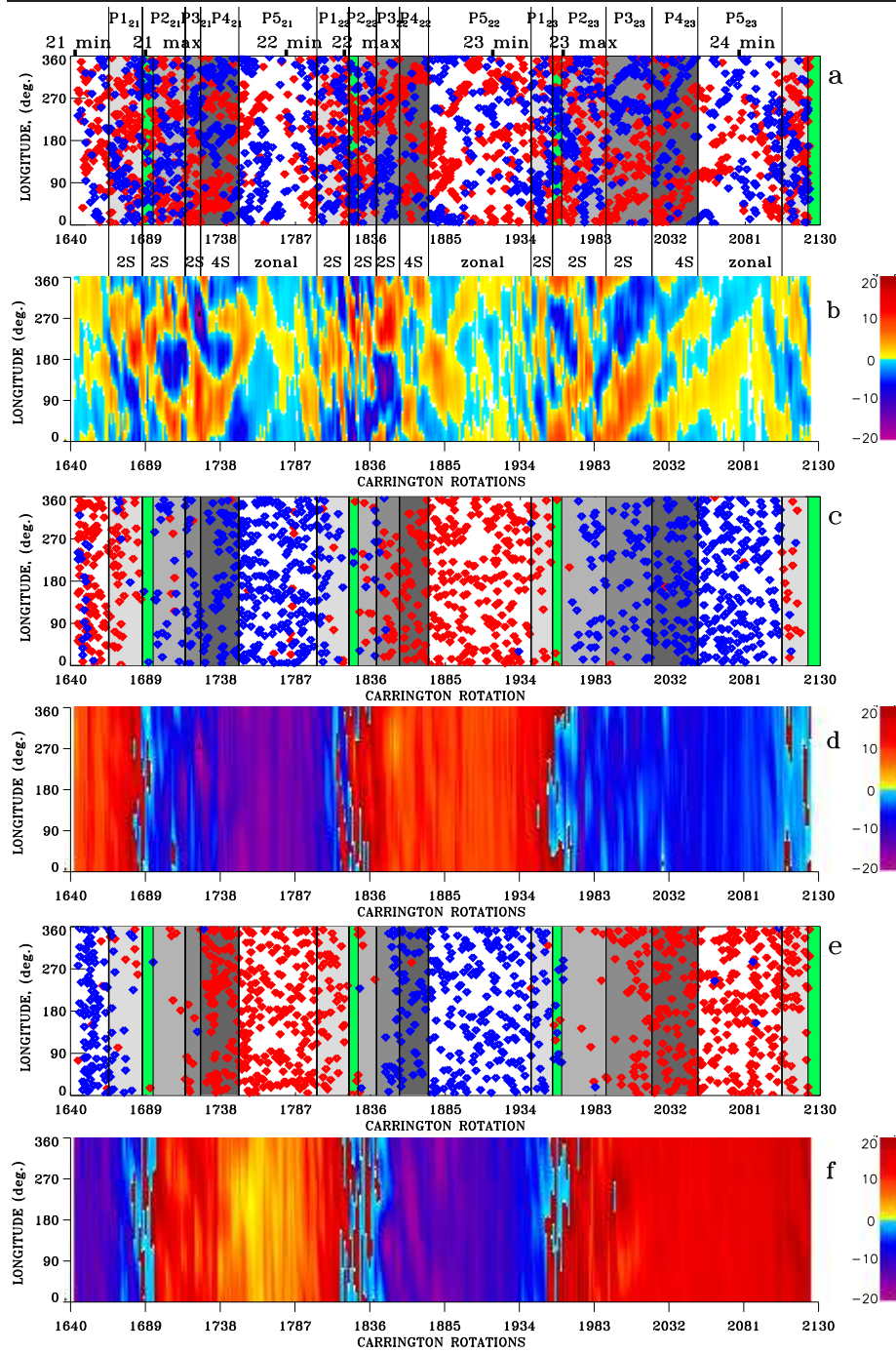


Figure 3. Longitudinal distributions of: (a) non-polar CHs associated with the positive-polarity (red) and negative-polarity (blue) magnetic fields; (b) GMF from -55° to $+55^\circ$ latitude for positive-polarity (red) and negative-polarity (blue) magnetic fields; (c) polar CHs associated with the positive-polarity (red) and negative-polarity (blue) photospheric magnetic fields in the North hemisphere; (d) GMF from $+55^\circ$ to $+70^\circ$ latitude for positive-polarity (red) and negative-polarity (blue) magnetic fields in the North hemisphere; (e) polar CHs associated with the positive-polarity (red) and negative-polarity (blue) photospheric magnetic fields in the South hemisphere; (f) GMF from -55° to -70° latitude for positive-polarity (red) and negative-polarity (blue) magnetic fields in the South hemisphere. Light-, mid-, and dark-grey mark the P1–P4 periods of the sectorial GMF structure domination. Green indicates the magnetic-field polarity reversals at the North and South poles.

phases are also clearly revealed in CH longitudinal location changes. During the late rise and maxima phases, the two-sector-polarity GMF structures are formed (Figure 3b). They are mostly occupied by positive- or by negative-polarity CHs (Figure 3a). The two-polarity structure in GMF and CHs is more pronounced during the declining phases in each cycle. The periods of reorganization in the GMF, characterized by the longitudinal rearrangement of magnetic-field polarity structures, are repeated by the changes in the locations of CHs associated with the positive- and negative-polarity photospheric magnetic fields. Reorganizations of the GMF and CH cluster structures occur simultaneously during a time interval of a few solar rotations. Old CH clusters disappear and a new set of CH clusters forms following the reorganizations in the GMF (Bilenko, 2004b; Bilenko, 2012).

The drifts in the GMF and CHs are the manifestation of the slower rotation at the rising phases and faster rotation at the declining phases. Wang and Sheeley (1990) proposed that rotation rate of CHs is determined by the centroidal latitude of the nonaxisymmetric flux. During the rising phase, CHs rotate at the slow rate of the decaying mid-latitude active-region magnetic fields. During the declining phase, the equatorward extensions of the polar CHs rotate at the faster rate of the low-latitude active-region remnants. According to our results, from Figure 2a we can see that during the rising phases, periods P1₂₁–P1₂₃, old-polarity polar CHs and low-latitude CHs, and the associated photospheric magnetic fields, are separated by the wave 1 CHs, that traced a new-polarity magnetic field. As a result, they rotate with different rates. In Figure 4, the examples of daily large-scale photospheric magnetic-field distributions and wave 1 coronal holes in the $\lambda = 10830 \text{ \AA}$, $\lambda = 284 \text{ \AA}$ lines, and soft X-ray observed in the North (Figure 4a–c) and the South (Figure 4d–f) hemispheres are presented. In the North hemisphere, negative-polarity (blue) magnetic-field structure separates positive-polarity (rose) polar and low-latitude magnetic fields (Figure 4a1, b1, c1). The associated coronal hole is shown in EUV and X-ray (Figure 4a2–a4, b2–b4, c2–c4). In the South hemisphere, positive-polarity magnetic-field structure separates negative-polarity south polar and low-latitude magnetic fields (Figure 4d1, e1, f1). The associated coronal hole is shown in EUV and X-ray (Figure 4d2–d4, e2–e4, f2–f4). These coronal holes have an extended shape in longitude.

During the declining and minimum phases, periods P4₂₁–P4₂₃, P5₂₁–P5₂₃, the polarity of polar and non-polar CHs, and associated photospheric magnetic fields, coincide. They create a common large-scale unipolar magnetic-field system. Therefore, the slow rotation rate of the polar regions affects the deceleration of the rotation of mid- and low-latitude photospheric magnetic fields and, consequently, the associated CHs. Figure 5 presents the examples of daily large-scale photospheric magnetic-field distributions and polar coronal-hole extensions in the $\lambda = 10830 \text{ \AA}$, $\lambda = 284 \text{ \AA}$ lines, and soft X-ray observed in the North (Figure 5a–c) and the South (Figure 5d–f) hemispheres. Positive-polarity magnetic-field structure is extended from the North pole to the South hemisphere high latitudes (Figure 5a1–c1). The associated coronal hole, the well known “Elephant trunk”, is seen in EUV and X-ray (Figure 5a2–a4, b2–b4, c2–c4). Negative-polarity magnetic-field structure is extended from the South

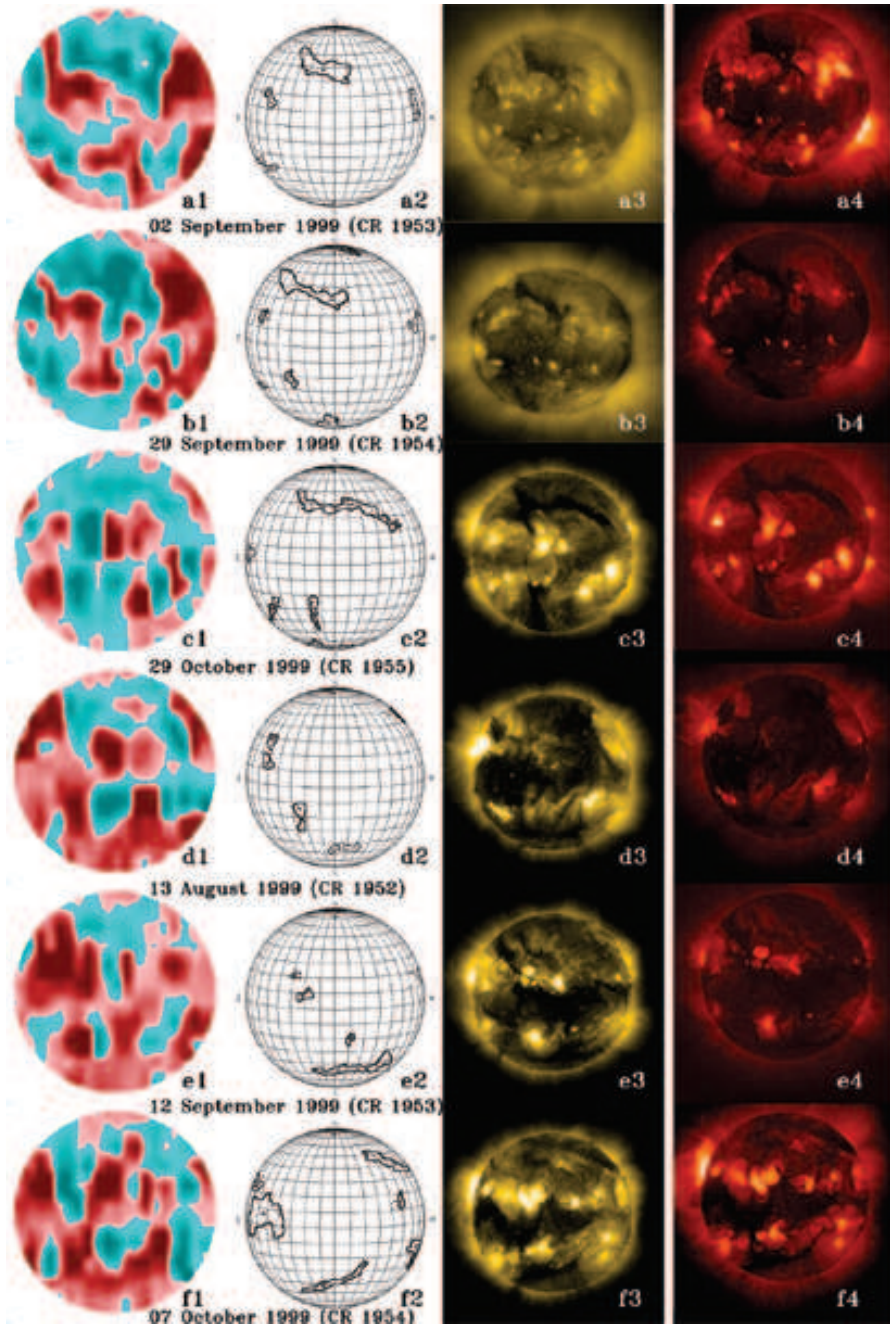


Figure 4. Large-scale photospheric positive-polarity (rose) and negative-polarity (blue) magnetic-field distributions (a1–f1) and wave 1 coronal holes in the $\lambda = 10830 \text{ \AA}$ (a2–f2), $\lambda = 284 \text{ \AA}$ (a3–f3) lines, and soft X-ray (a4–f4) observed in the North (a–c) and South (d–f) hemispheres.

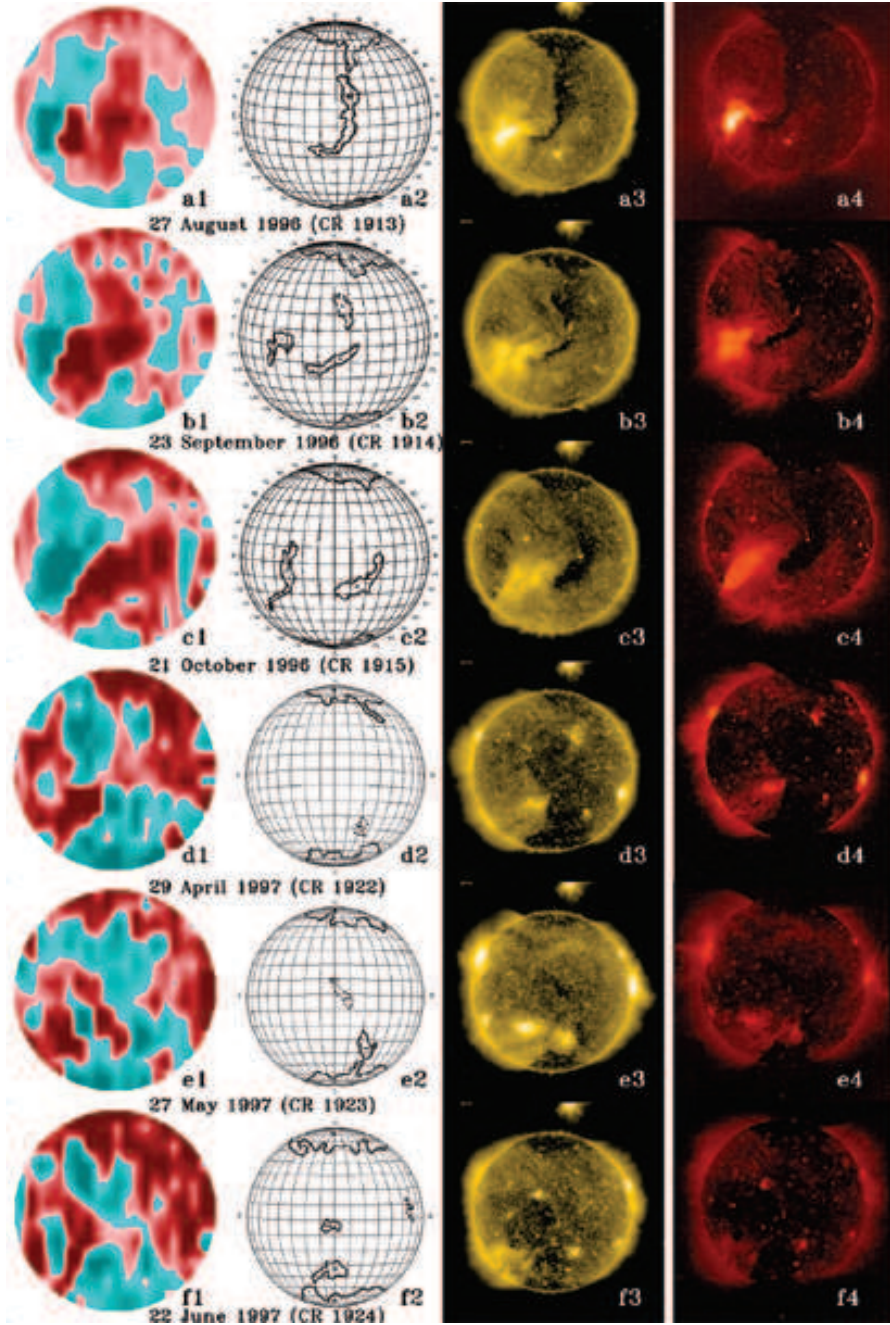


Figure 5. Large-scale photospheric positive-polarity (rose) and negative-polarity (blue) magnetic-field distributions (a1–f1) and polar coronal-hole extensions in the $\lambda = 10830 \text{ \AA}$ (a2–f2), $\lambda = 284 \text{ \AA}$ (a3–f3) lines, and soft X-ray (a4–f4) observed in the North (a–c) and South (d–f) hemispheres.

pole to the North hemisphere (Figure 5d1–f1). The associated coronal hole is shown in EUV and X-ray (Figure 5d2–d4, e2–e4, f2–f4). These coronal holes have an extended shape in latitude. The polar CH extensions change their shape from CR to CR. The polar CH extensions to low latitudes rotate with the polar CH rate, even after they are disconnected (Zhao, Hoeksema, and Scherrer, 1999). The large-scale magnetic-field structures are more stable.

Fox, McIntosh, and Wilson (1998) found that the polar CH evolution during solar activity cycles was closely related to the polar magnetic fields. Studying the polar magnetic-field reversals in cycles 21 and 22, they suggested that the polar reversals originated from the global processes rather than from local magnetic flux dynamics. In Figure 3c, the longitudinal distribution of the North polar CHs is presented and in Figure 3d, the time-longitude distribution of the strength and polarity of the GMF for latitudes from 55° to 70° is shown. In Figure 3e, the longitudinal distribution of the South polar CHs is presented and in Figure 3f the time-longitude distribution of the strength and polarity of the GMF is shown for latitudes from -55° to -70° .

In Figures 3a and b, the polarity clusters of CHs and their association with the GMF distribution and evolution are seen. To show the latitudinal distribution of CHs and associated GMF during each period, the polar projection plots were created. Polar projection distributions of CHs associated with the positive-polarity (red) and negative-polarity (blue) photospheric magnetic fields and the GMF are presented in Figures 6–9 seen from the North pole (left side panels) and South pole (right side panels) for different periods in cycles 21–23.

During the first periods (P1₂₁–P1₂₃), old-polarity polar CHs still dominate at the poles, but CHs associate with a new-polarity photospheric magnetic fields are already at high latitudes and they are located at preferred longitudes. The sectorial structure is not completely established. The changes in GMF structure and CH distribution are rather chaotic (Figures 3a, b, 6a1, 6a2–8a1, 8a2).

During the periods P2₂₁–P2₂₃, P3₂₁–P3₂₃ the new-polarity polar CHs are already completely formed. Mid- and low-latitude CHs reveal a two-sectorial distribution. The CH distribution coincides with that of the GMF. Such a longitudinal distribution of the GMF and CHs indicates the increased role of the axisymmetric GMF components at that time. The changes in the distribution of CHs associated with positive- and negative-polarity magnetic fields coincides with the redistribution of the GMF (Figures 1e, 3a, b, and 6b1, 6b2, 6c1, 6c2–8b1, 8b2, 8c1, 8c2). During P3 periods, the two-sectorial structure is more pronounced in each cycle.

During the periods P4₂₁–P4₂₃, a four-sector structure is formed. The sectorial and zonal harmonic spectral sum are nearly equal (Figures 1a, b, 3a, b and 6d1, 6d2–8d1, 8d2).

During the periods P5₂₁–P5₂₃, the time of the zonal GMF structure domination, the polarity of mid-latitude CHs matches that of the polar CHs in the corresponding hemisphere. The polar and non-polar CHs are associated with the GMF of the same polarity in each hemisphere (Figure 9). They reflect the zonal structure of the GMF with $m=0$, $n=1$. The residuals of the sectorial structure can be seen in low-latitude GMF and CHs (Figures 3a, b, and 9). The large extensions are developed from the polar CHs to low latitudes at that time (Figure 5). The life-time of some extensions exceeds several CRs.

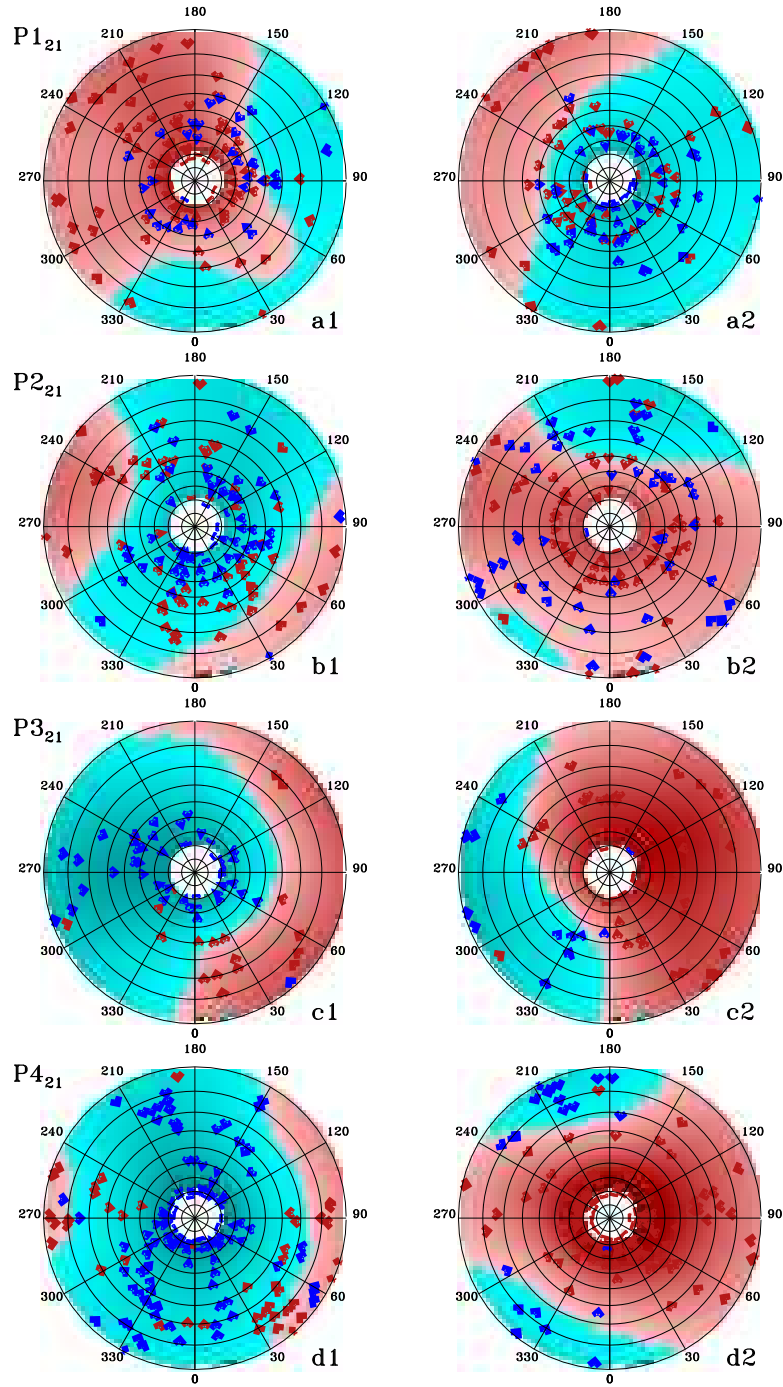


Figure 6. The polar projections of the distributions of CHs associated with positive-polarity (red) and negative-polarity (blue) photospheric magnetic fields and GMF seen from the North pole (left side panels) and South pole (right side panels) for periods $P1_{21}$ – $P4_{21}$ in cycle 21.

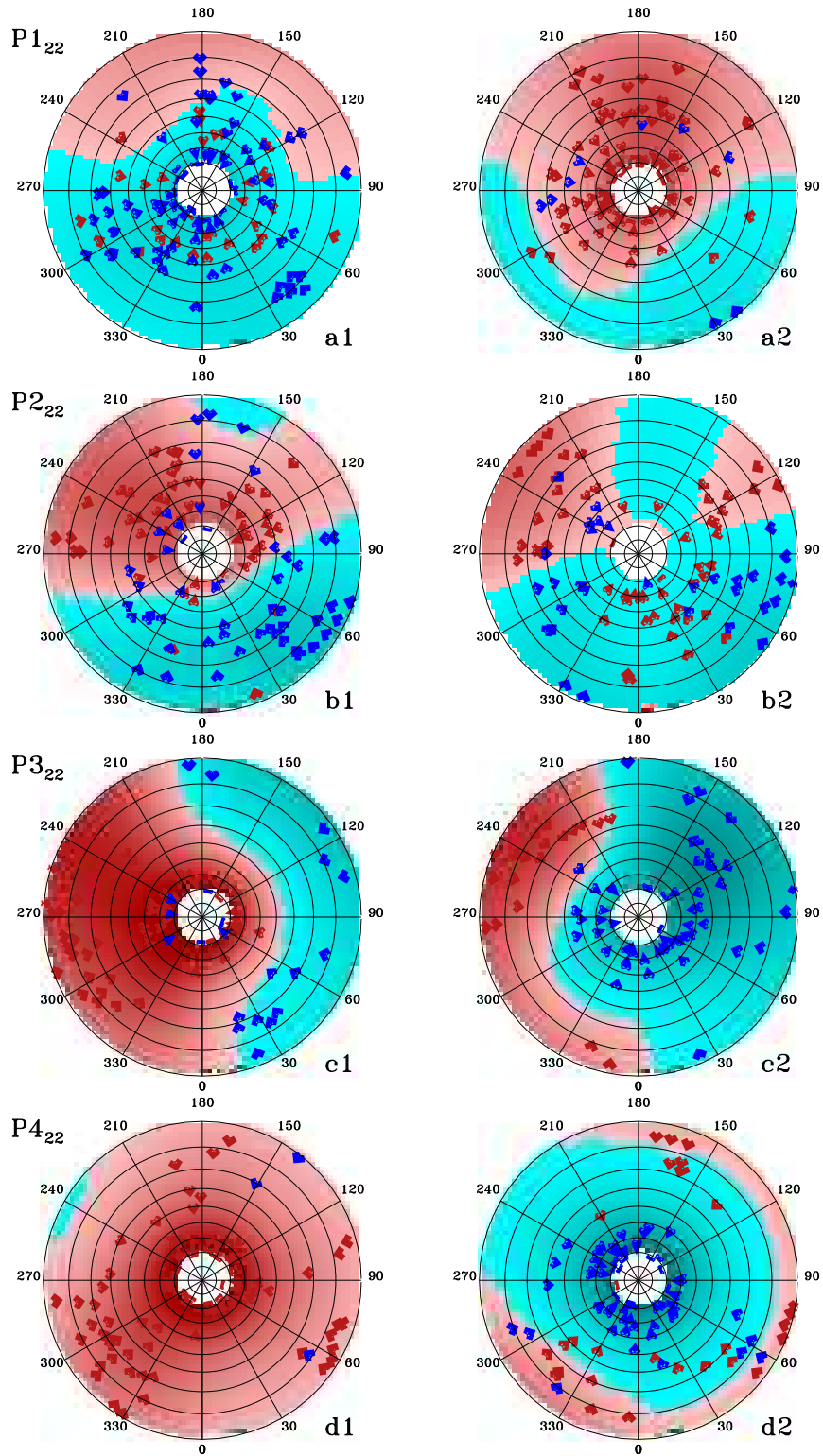


Figure 7. The polar projections of the distributions of CHs associated with positive-polarity (red) and negative-polarity (blue) photospheric magnetic fields and GMF seen from the North pole (left side panels) and South pole (right side panels) for periods $P1_{22} - P4_{22}$ in cycle 22.

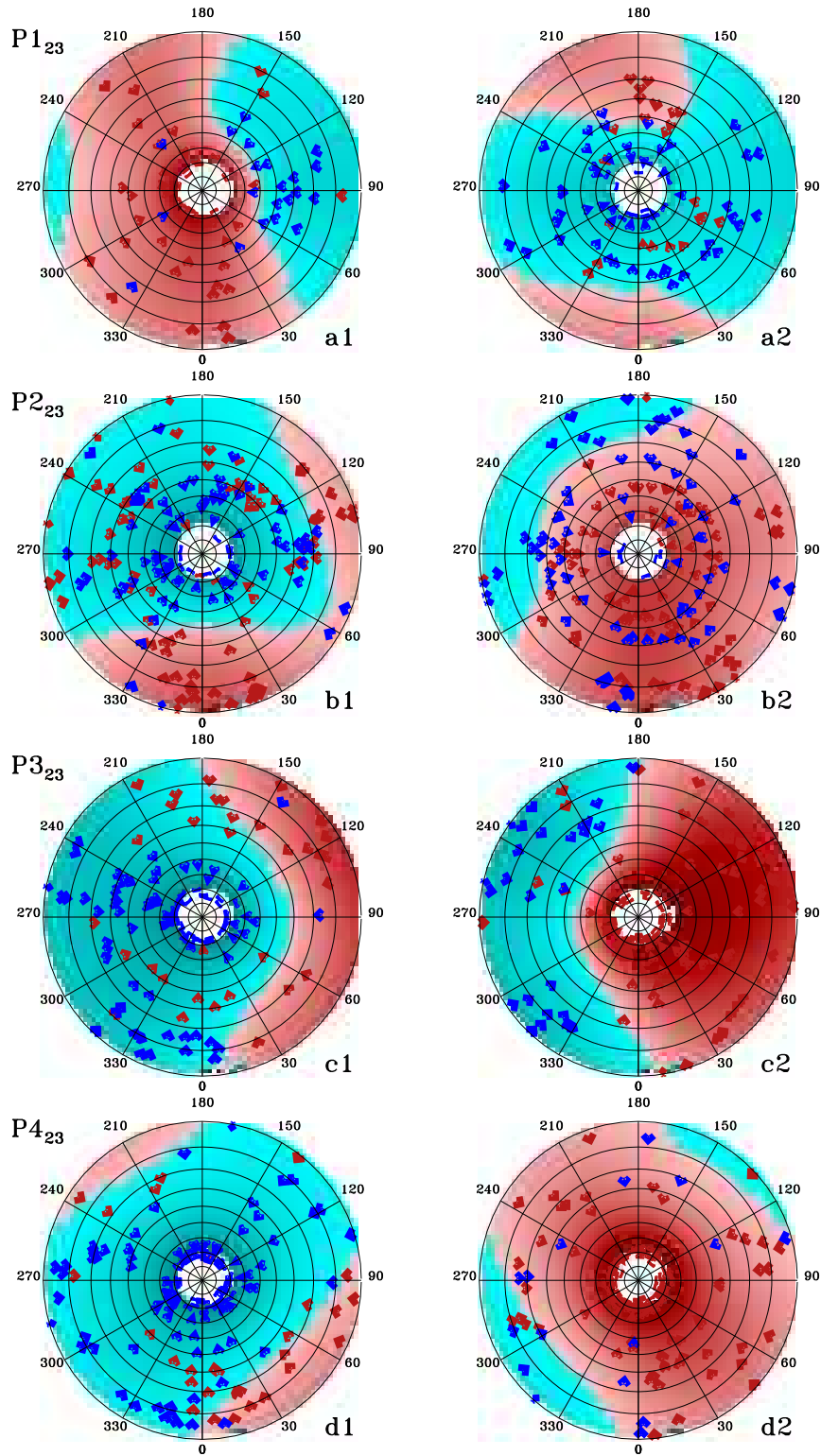


Figure 8. The polar projections of the distributions of CHs associated with positive-polarity (red) and negative-polarity (blue) photospheric magnetic fields and GMF seen from the North pole (left side panels) and South pole (right side panels) for periods $P1_{23}$ – $P4_{23}$ in cycle 23.

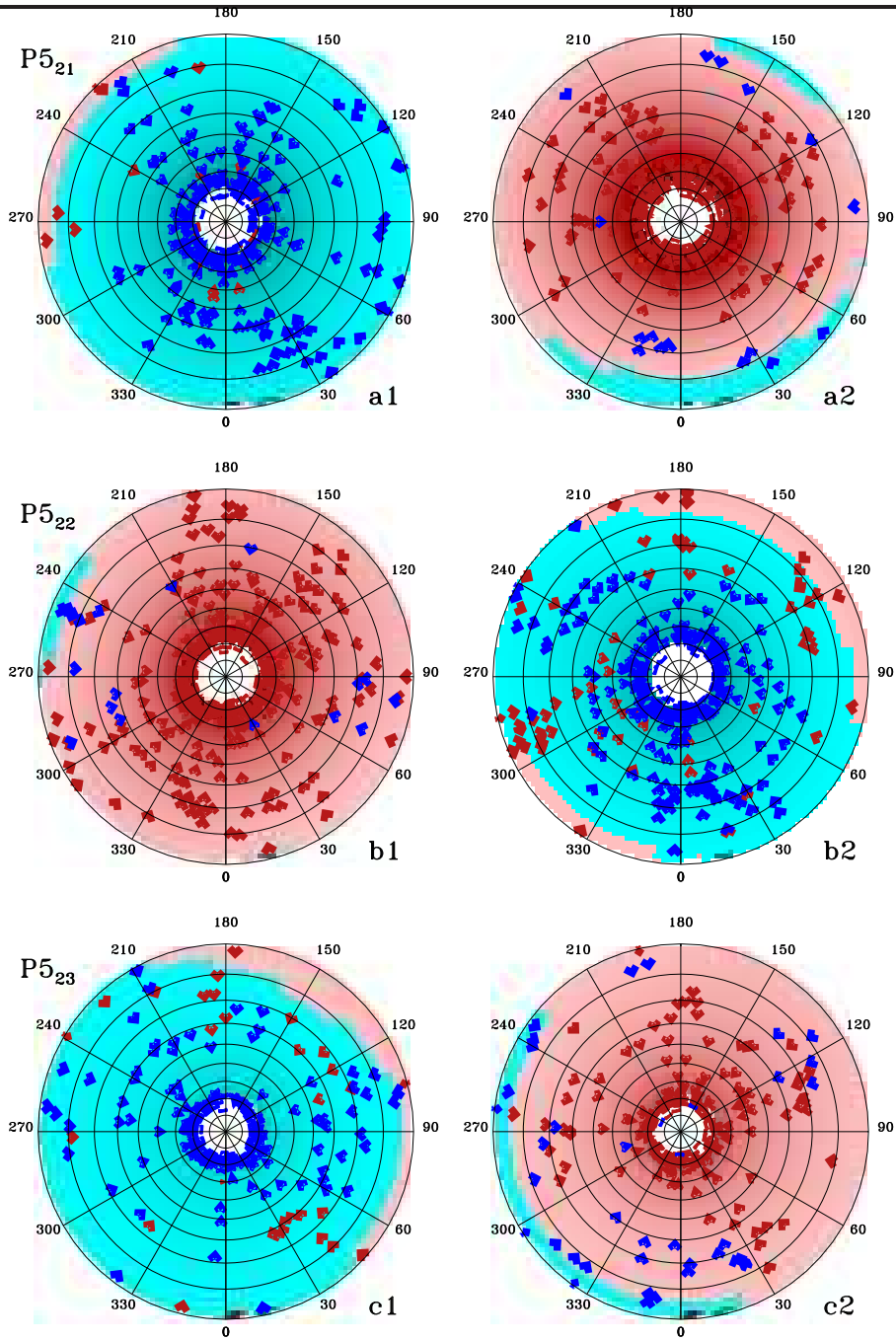


Figure 9. The polar projections of the distributions of CHs associated with positive-polarity (red) and negative-polarity (blue) photospheric magnetic fields and GMF seen from the North pole (left side panels) and South pole (right side panels) during the zonal GMF structure domination periods P5₂₁–P5₂₃ in cycles 21–23.

6. Coronal Hole Parameters and the Global Magnetic Field

As can be seen from Figure 10, showing the polar CH parameters as well as the positive- and negative-polarity and their absolute value sum of CR-averaged GMF evolution, the number of polar CHs and their latitudinal and longitudinal extensions, areas, and magnetic flux are maximal during the zonal GMF structure (P5₂₁–P5₂₃). Non-polar GMF is minimal at that time. There are additional peaks in polar CH latitudinal and longitudinal extensions, areas, and magnetic flux during the end of period P3₂₂ in cycle 22, and during periods P2₂₃–P4₂₃ in cycle 23. Magnetic-field strength reaches a maximum in the period P5₂₁ (zonal GMF structure domination) in cycle 21, and to the period P3 in cycles 22 and 23. During polar magnetic-field reversals, the number of polar CHs is minimal and all CH parameters are also at the lowest level (Figure 10). The polar magnetic-field sign changes are characterized by a decrease in the GMF strength, and the magnitude of the sectorial components of the GMF (Figure 1).

The number of non-polar CHs and all their parameters are maximal during the sectorial GMF structure domination, and they are at a low level at the time of the zonal GMF structure (Figure 11).

The total CH number changes little during cycles 21–23 (Figure 12). This is associated with a phase shift in the variation of the polar and non-polar CH numbers by approximately half the cycle duration. The polar CHs dominate in total CH longitudinal extension evolution and area. The average total CH latitudinal extensions change rather chaotically. The total CH flux and magnetic-field strength in CHs associated with the positive- and negative-polarity photospheric magnetic fields is lower in cycle 23. This is probably due to a decrease in the strength of the polar magnetic field in cycle 23 (Wang, Robbrecht, and Sheeley, 2009; Tlatov, Tavastsherna, and Vasil’eva, 2014).

7. Conclusion

The comparison of CHs and GMF shows that the GMF determines the CH evolution in cycles 21–23.

Comparison of the CH and GMF longitudinal distributions shows that the CH cluster structure completely coincides with the GMF longitudinal distribution. Positive-polarity CH locations coincide with positive-polarity GMF and negative-polarity CH locations coincide with negative-polarity GMF. CH longitudinal distributions follow all configurations in the GMF. Reorganizations of the GMF and CH cluster structures occur simultaneously during a time interval of a few solar rotations.

CHs are divided into two groups: polar and non-polar CHs according to their latitudinal locations. The number of polar CHs and their latitudinal and longitudinal extensions, areas, and magnetic flux are maximal during the zonal GMF structure. The number of non-polar CHs and all their parameters are maximal during the sectorial GMF structure domination. The total CH number changes little during cycles 21–23. This is due to an approximately half a cycle phase shift in the polar and non-polar CH numbers.

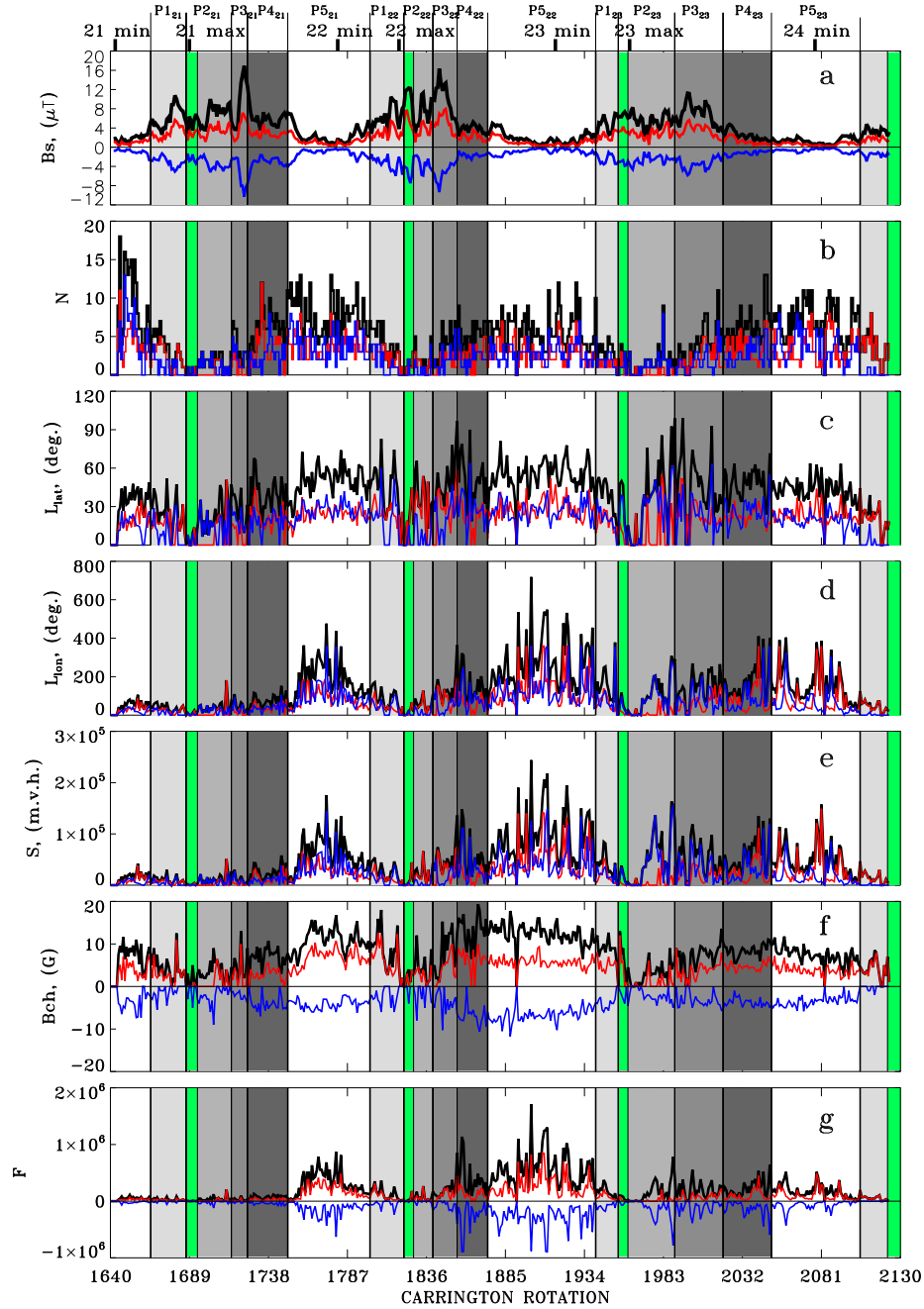


Figure 10. (a) Positive-polarity (red) and negative-polarity (blue) CR-averaged GMF and their absolute value sum (black); (b) polar CH numbers; (c) polar CH latitudinal extension; (d) polar CH longitudinal extension; (e) polar CH area; (f) polar CH-associated photospheric magnetic field; (g) polar CH-associated magnetic flux. Red denotes the parameters of CHs associated with the positive-polarity magnetic fields. Blue denotes the parameters of CHs associated with the negative-polarity magnetic fields. Light-, mid-, and dark-grey mark the P1–P4 periods of the sectorial GMF structure domination. Green indicates the magnetic-field polarity reversals at the North and South poles.

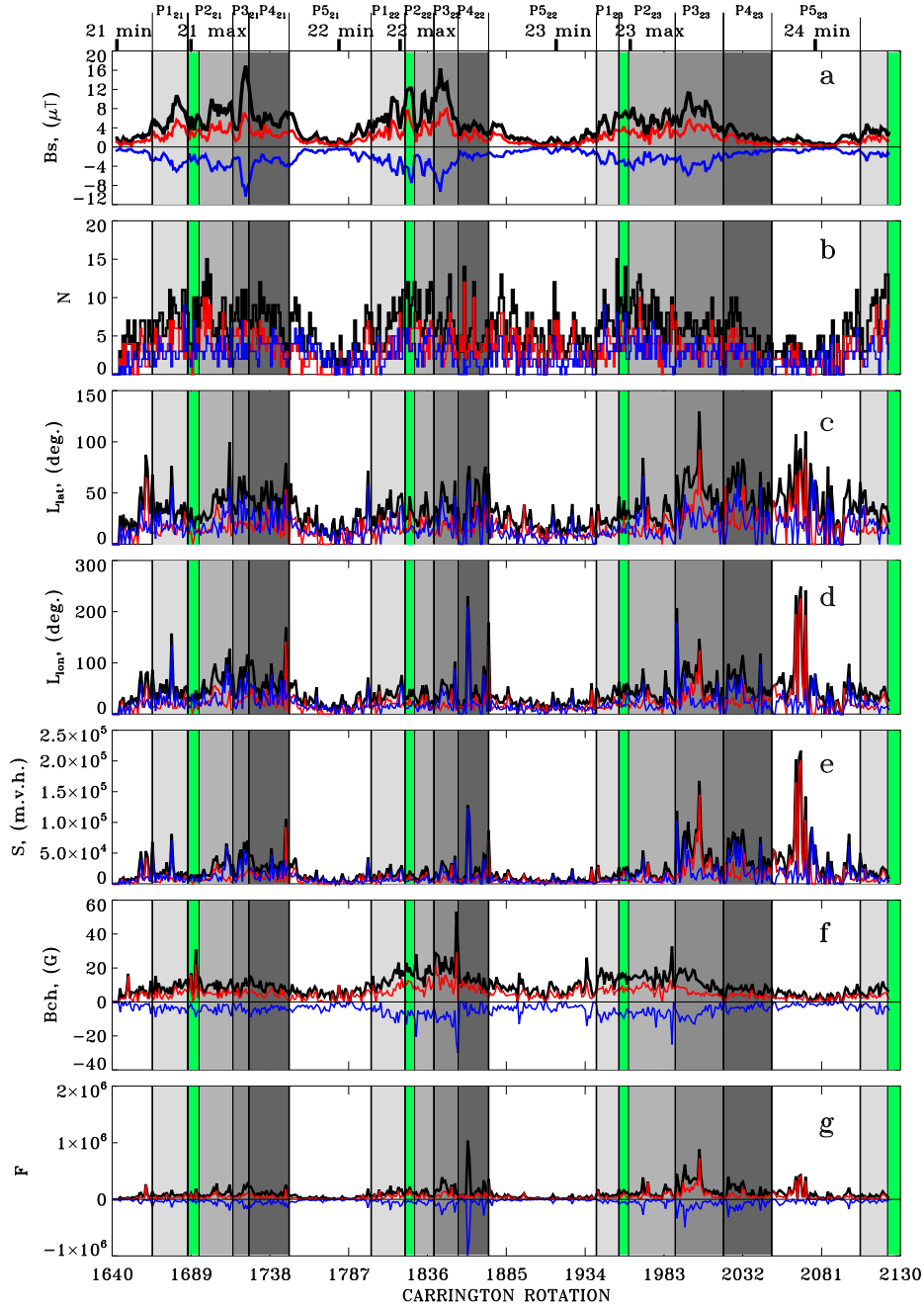


Figure 11. (a) Positive-polarity (red) and negative-polarity (blue) CR-averaged GMF and their absolute value sum (black); (b) non-polar CH numbers; (c) non-polar CH latitudinal extension; (d) non-polar CH longitudinal extension; (e) non-polar CH area; (f) non-polar CH-associated photospheric magnetic field; (g) non-polar CH-associated magnetic flux. Red denotes the parameters of CHs associated with the positive-polarity magnetic fields. Blue denotes the parameters of CHs associated with the negative-polarity magnetic fields. Light-, mid-, and dark-grey mark the P1–P4 periods of the sectorial GMF structure domination. Green indicates the magnetic-field polarity reversals at the North and South poles.

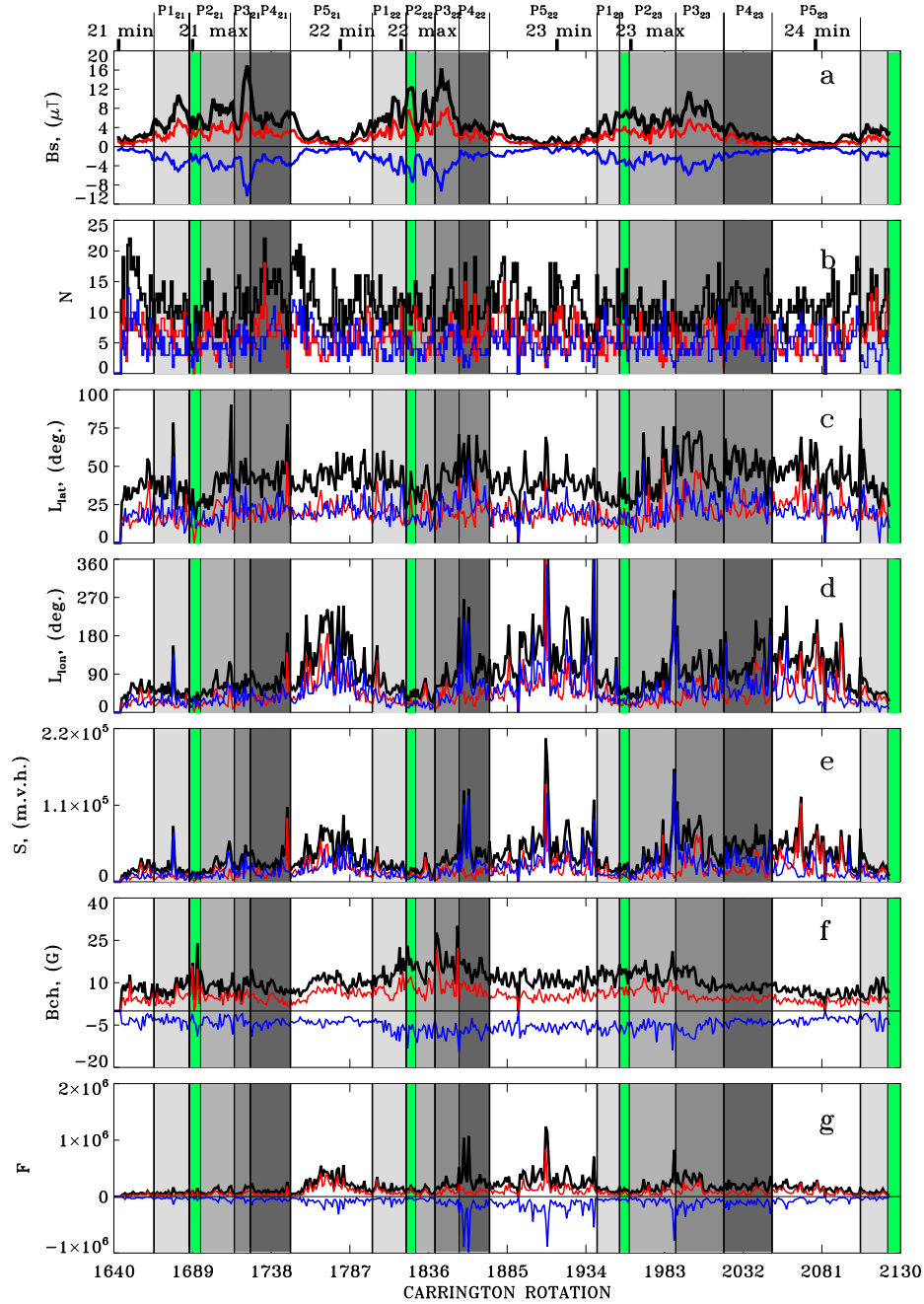


Figure 12. (a) Positive-polarity (red) and negative-polarity (blue) CR-averaged GMF and their absolute value sum (black); (b) CH numbers; (c) CH latitudinal extension; (d) CH longitudinal extension; (e) CH area; (f) CH-associated photospheric magnetic field; (g) CH-associated magnetic flux. In (b) - (g) red denotes the parameters of CHs associated with the positive-polarity magnetic fields. Blue denotes the parameters of CHs associated with the negative-polarity magnetic fields. Light-, mid-, and dark-grey mark the P1–P4 periods of the sectorial GMF structure domination. Green indicates the magnetic-field polarity reversals at the North and South poles.

Two different type waves of non-polar coronal holes were revealed from their latitudinal distribution. The first one (waves 1) are short poleward waves. They trace the poleward motion of the unipolar photospheric magnetic fields from approximately 35° to the associated pole in each hemisphere and the redevelopment of a new-polarity polar CH. Although they started the poleward movement before the change of the polar magnetic field in the associated hemisphere, they reached the pole after the polar reversal.

The other type are non-polar CH waves (waves 2) that form two sinusoidal branches. One branch is associated with the positive-polarity magnetic fields and the other with that of the negative-polarity. The complete period of the wave 2 CH waves was equal to ≈ 268 CRs (≈ 22 years). The branches were in anti phase in each cycle. Wave 2 CHs reached the highest latitudes and polar CH regions at the time of the end of old-polarity magnetic-field domination at the associated pole, late at the declining phases. The latitude-location cycle changes of the wave 2 CHs coincided with that of the axisymmetric component of the solar dipole. When two branches of positive- and negative-polarity magnetic fields, traced by wave 2 CHs, went down below $\approx \pm 35^\circ$ latitude, the sectorial structure of the GMF was established. When both branches were above $\approx \pm 35^\circ$ latitude, the zonal structure was observed. The polarity of CH-associated magnetic fields matched the polarity of the polar regions in the hemisphere that time.

The drifts in the GMF and CHs longitudinal distributions are the manifestation of the slower rotation at the rising phases and faster rotation at the declining phases. During the rising phases, old-polarity polar and low-latitude CHs, and the associated photospheric magnetic fields, were separated by the wave 1 CHs, that traced a new-polarity magnetic field. At the late declining and minima phases, the polarity of the polar and non-polar CHs, and the associated photospheric magnetic fields, coincided. They created a common large-scale unipolar magnetic-field system. Therefore, slow rotation rate of the polar regions affected the deceleration of the rotation of mid- and low-latitude photospheric magnetic fields and, consequently, the associated CHs.

Acknowledgments We acknowledged Dr. Tlatov A. G. and all Kislovodsk Mountain Astronomical Station of Pulkovo Observatory team for the catalog of coronal holes used in this study.

Wilcox Solar Observatory data used in this study was obtained via the web site <http://wso.stanford.edu> at 2015:02:26 00:54:03 PST courtesy of J.T. Hoeksema. The Wilcox Solar Observatory is currently supported by NASA.

NSO/Kitt Peak data used here are produced cooperatively by NSF/NOAO, NASA/GSFC, and NOAA/SEL.

The *Yohkoh* mission was developed and launched by ISAS/JAXA, Japan, with NASA and SERC/PPARC (UK) as international partners. This work made use of the *Yohkoh* Legacy data Archive at Montana State University, which is supported by NASA.

SOHO/EIT data were used. SOHO is a project of international cooperation between ESA and NASA.

References

- Altschuler, M.D., Newkirk, G.: 1969, Magnetic fields and the structure of the solar corona. I: methods of calculating coronal fields. *Solar Phys.* **9**, 131. DOI. [Altschuler1969]

- Altschuler, M.D., Trotter, D.E., Newkirk, G.J., Howard, R.: 1975, Tabulation of the harmonic coefficients of the solar magnetic fields. *Solar Phys.* **41**, 225. DOI. [Altschuler1975]
- Altschuler, M.D., Levine, R.H., Stix, M., Harvey, J.: 1977, High resolution mapping of the magnetic field of the solar corona. *Solar Phys.* **51**, 345. DOI. [Altschuler1977]
- Belenko, I.A.: 2001, Coronal hole evolution during 1996/1999. *Solar Phys.* **199**, 23. DOI. [Belenko2001]
- Bilenko, I.A.: 2002, Coronal holes and the solar polar field reversal. *Astron. Astrophys.* **396**, 657. DOI. [Bilenko2002]
- Bilenko, I.A.: 2004a, Formation and evolution of different type coronal holes. In: Stepanov, A.V., Benevolenskaya, E.E., Kosovichev, A.G. (eds.) *Multi-wavelength investigations of solar activity*, Proceedings IAU Symposium No. 223, ???, 373. DOI. [Bilenko2004a]
- Bilenko, I.A.: 2004b, Longitudinal distribution of coronal holes during 1976-2002. *Solar Phys.* **221**, 261. DOI. [Bilenko2004b]
- Bilenko, I.A.: 2005, Identification of the sources of the high-speed and low-speed streams of the solar wind. *Int. J. Geomagn. Aeron.* **6**, GI1009. DOI. [Bilenko2005]
- Bilenko, I.A.: 2012, Statistical analysis of the structure and dynamics of coronal hole magnetic fields. In: Ballester, P., Egret, D., Lorente, N.P.F. (eds.) *Astronomical data analysis software and systems XXI*, ASP, Vol. 461, ???, 479. [Bilenko2012]
- Bilenko, I.A.: 2014, Influence of the solar global magnetic-field structure evolution on CMEs. *Solar Phys.* **289**, 4209. DOI. [Bilenko2014]
- Bohlin, J.D., Sheeley, N.R.J.: 1978, Extreme ultraviolet observations of coronal holes. II - Association of holes with solar magnetic fields and a model for their formation during the solar cycle. *Solar Phys.* **56**, 125. DOI. [Bohlin1978]
- Bravo, S., Stewart, G.A.: 1997, Fast and slow wind from solar coronal holes. *Astrophys. J.* **489**, 992. [Bravo1997]
- Bumba, V., Klvaňa, M., Sýkora, J.: 1995, Coronal holes and their relation to the background and local magnetic fields. *Astron. Astrophys.* **298**, 923. [Bumba1995]
- Chapman, S., Bartels, J.: 1940, *Geomagnetism*, Geomagnetism, Oxford Univ. Press., 1940, ????. [Chapman1940]
- Delaboudinière, J.-P., Artzner, G.E., Brunaud, J., Gabriel, A.H., Hochedez, J.F., Millier, F., Song, X.Y., Au, B., Dere, K.P., Howard, R.A., Kreplin, R., Michels, D.J., Moses, J.D., Defise, J.M., Jamar, C., Rochus, P., Chauvineau, J.P., Marioge, J.P., Catura, R.C., Lemen, J.R., Shing, L., Stern, R.A., Gurman, J.B., Neupert, W.M., Maucherat, A., Clette, F., Cugnon, P., van Dessel, E.L.: 1995, EIT: extreme-ultraviolet imaging telescope for the SOHO mission. *Solar Phys.* **162**, 291. DOI. [Delaboudiniere1995]
- Dorotovič, I.: 1996, Area of polar coronal holes and sunspot activity: years 1939-1993. *Solar Phys.* **167**, 419. DOI. [Dorotovic1996]
- Fox, P., McIntosh, P., Wilson, P.R.: 1998, Coronal holes and the polar field reversals. *Solar Phys.* **177**, 375. DOI. [Fox1998]
- Harvey, K.L., Recely, F.: 2002, Polar coronal holes during cycles 22 and 23. *Solar Phys.* **211**, 31. DOI. [Harvey2002]
- Harvey, K.L., Sheeley, N.R.J., Harvey, J.W.: 1982, Magnetic measurements of coronal holes during 1975-1980. *Solar Phys.* **79**, 149. DOI. [Harvey1982]
- Hess Webber, S.A., Karna, N., Pesnell, W.D., Kirk, M.S.: 2014, Areas of polar coronal holes from 1996 through 2010. *Solar Phys.* **289**, 4047. DOI. [Hess2014]
- Hoeksema, J.T.: *Structure and evolution of the large scale solar and heliospheric magnetic fields*, Ph. D. Thesis, Stanford Univ., CA., 1984. [Hoeksema1984]
- Hoeksema, J.T., Scherrer, P.H.: 1986, An atlas of photospheric magnetic field observations and computed coronal magnetic fields: 1976-1985. *Solar Phys.* **105**, 205. DOI. [Hoeksema1986]
- Hoeksema, J.T., Scherrer, P.H.: 1988, An atlas of photospheric magnetic field observations and computed coronal magnetic fields: 1976-1985. *Solar - Geophysical Data (SGD)* **105**, no. 383. [Hoeksema1988]
- Ikhsanov, R.N., Ivanov, V.G.: 1999, Properties of space and time distribution of solar coronal holes. *Solar Phys.* **188**, 245. DOI. [Ikhsanov1999]
- Ikhsanov, R.N., Tavastsherna, K.S.: 2013, High-latitude coronal holes and polar faculae in the 21st-23rd solar activity cycles. *Geomagnetism and Aeronomy* **53**, 896. DOI. [Ikhsanov2013]
- Ikhsanov, R.N., Tavastsherna, K.S.: 2015, Latitudetemporal evolution of coronal holes in cycles 21-23. *Geomagnetism and Aeronomy* **55**, 877. DOI. [Ikhsanov2015]
- Insley, J.E., Moore, V., Harrison, R.A.: 1995, The differential rotation of the corona as indicated by coronal holes. *Solar Phys.* **160**, 1. DOI. [Insley1995]

- Ivanov, E.V., Obridko, V.N.: 2014, Role of the large-scale solar magnetic field structure in the global organization of solar activity. *Geomagnetism and Aeronomy* **54**, 996. DOI. [Ivanov2014]
- Levine, R.H.: 1977, Evolution of photospheric magnetic field patterns during SKYLAB. *Solar Phys.* **54**, 327. DOI. [Levine1977]
- McIntosh, P.S., Thompson, R.J., Willock, E.C.: 1992, A 600-day periodicity in solar coronal holes. *Nature* **360**, 322. DOI. [McIntosh1992]
- Miralles, M.P., Cranmer, S.R., Kohl, J.L.: 2001, Ultraviolet coronagraph spectrometer observations of a high-latitude coronal hole with high oxygen temperatures and the next solar cycle polarity. *Astrophys. J.* **560**, L193. DOI. [Miralles2001]
- Miralles, M.P., Cranmer, S.R., Kohl, J.L.: 2002, Cyclic variation in the plasma properties of coronal holes. In: Wilso, A. (ed.) *SOHO 11. From solar min to max: half a solar cycle with SOHO*, ESA SP-508, ???, 351. [Miralles2002]
- Miralles, M.P., Cranmer, S.R., Kohl, J.L.: 2006, Coronal hole properties during the first decade of UVCS/SOHO. In: Lacoste, H. (ed.) *SOHO 17 - 10 years of SOHO and beyond*, ESA SP-617, ESTEC, The Netherlands, ???, 15. [Miralles2006]
- Nolte, J.T., Krieger, A.S., Timothy, A.F., Gold, R.E., Roelof, E.C., Vaiana, G., Lazarus, A.J., Sullivan, J.D., McIntosh, P.S.: 1976, Coronal holes as sources of solar wind. *Solar Phys.* **46**, 303. DOI. [Nolte1976]
- Obridko, V.N., Shelting, B.D.: 1989, Coronal holes as indicators of large-scale magnetic fields in the corona. *Solar Phys.* **124**, 73. DOI. [Obridko1989]
- Obridko, V.N., Shelting, B.D., Livshits, I.M.: 2011, Relationship between the parameters of coronal holes and high-speed solar wind streams over an activity cycle. *Solar Phys.* **270**, 297. DOI. [Obridko2011]
- Sanchez-Ibarra, A., Barraza-Paredes, M.: 1992, *Catalog of coronal holes, 1970-1991, report UAG-102*, Boulder: World Data Center A for solar-terrestrial physics, National Geophysical Data Center, 1992, ???, [Sanchez1992]
- Schatten, K.H., Wilcox, J.M., Ness, N.F.: 1969, A model of interplanetary and coronal magnetic fields. *Solar Phys.* **6**, 442. DOI. [Schatten1969]
- Stix, M.: 1977, Coronal holes and the large-scale solar magnetic field. *Astron. Astrophys.* **59**, 73. [Stix1977]
- Tavastsherna, K.S., Polyakow, E.V.: 2014, Coronal holes, large-scale magnetic field, and activity complexes in solar cycle 23. *Geomagnetism and Aeronomy* **54**, 953. DOI. [Tavastsherna2014]
- Tavastsherna, K.S., Tlatov, A.G.: 2004, Properties of the magnetic field in the coronal holes in solar cycle 23. In: Stepanov, A.V., Benevolenskaya, E.E., Kosovichev, A.G. (eds.) *Multi-wavelength investigations of solar activity*, IAU Symposium No. 223, ???, 301. DOI. [Tavastsherna2004]
- Temmer, M., Vršnak, B., Veronig, A.M.: 2007, Periodic appearance of coronal holes and the related variation of solar wind parameters. *Solar Phys.* **241**, 371. DOI. [Temmer2007]
- Timothy, A.F., Krieger, A.S., Vaiana, G.S.: 1975, The structure and evolution of coronal holes. *Solar Phys.* **42**, 135. DOI. [Timothy1975]
- Tlatov, A., Tavastsherna, K., Vasil'eva, V.: 2014, Coronal holes in solar cycles 21 to 23. *Solar Phys.* **289**, 1349. DOI. [Tlatov2014]
- Tsuneta, S., Acton, L., Bruner, M., Lemen, J., Brown, W., Carvalho, R., Catura, R., Freeland, S., Jurcevich, B., Morrison, M., Ogawara, Y., Hirayama, T., Owens, J.: 1991, The soft X-ray telescope for the SOLAR-A mission. *Solar Phys.* **136**, 37. DOI. [Tsuneta1991]
- Varsik, J.R., Wilson, P.R., Li, Y.: 1999, High-resolution studies of the solar polar magnetic fields. *Solar Phys.* **184**, 223. DOI. [Varsik1999]
- Waldmeier, M.: 1981, Cyclic variations of the polar coronal hole. *Solar Phys.* **70**, 251. DOI. [Waldmeier1981]
- Wang, Y.M., Sheeley, N.R.J.: 1990, Magnetic flux transport and the sunspot-cycle evolution of coronal holes and their wind streams. *Astrophys. J.* **365**, 372. DOI. [Wang1990]
- Wang, Y.-M., Robbrecht, E., Sheeley, N.R.J.: 2009, On the weakening of the polar magnetic fields during solar cycle 23. *Astrophys. J.* **707**, 13721386. DOI. [Wang2009]
- Webb, D.F., Davis, J.M., McIntosh, P.S.: 1984, Observations of the reappearance of polar coronal holes and the reversal of the polar magnetic field. *Solar Phys.* **92**, 109. DOI. [Webb1984]
- Zhao, X.P., Hoeksema, J.T., Scherrer, P.H.: 1999, Changes of the boot-shaped coronal hole boundary during whole sun month near sunspot minimum. *J. Geophys. Res.* **104**, 9735. DOI. [Zhao1999]